OR-05-4-2

Methods for Calculating the Effective Solar-Optical Properties of a Venetian Blind Layer

Darryl S. Yahoda

John L. Wright, PhD, PEng
Member ASHRAE

ABSTRACT

Window solar gain can strongly influence building energy consumption, peak loads, and comfort. Shading devices are routinely used to control solar gain. The use of venetian blinds is particularly common. There is a strong need for models that can accurately simulate this type of device. As a first step, previous research focused on the mechanisms of longwave radiant exchange. Methods were presented by which spatially averaged optical properties (referred to as "effective" optical properties) can be calculated. An enclosure model was formulated to model the interaction of radiation with the slat surfaces. This optical model allows the venetian blind to be treated as a planar, homogeneous "black-box" layer in a series of glazing layers and, coupled with the appropriate convection model, can be incorporated within a standard one-dimensional center-glass heat transfer analysis. In conjunction with the longwave analysis, the current study deals with the mechanisms of solar radiant exchange. Methods, based on geometric considerations and fundamental radiation analysis, are presented for determining the shading layer's effective optical properties with respect to the beam component of incident solar radiation—at any angle of incidence. Both specular and diffuse reflection at the slat surfaces is included. The performance of these effective properties is demonstrated and discussed in terms of expected results and compared with other models and experimental results found in the literature.

INTRODUCTION

One strategy for controlling solar heat gain through windows is the use of a slat-type shading device, in particular, a venetian blind, which can act as an adjustable barrier to solar transmission. The selection of the correct shading system requires information on the optical characteristics of the shading system as well as its influence on heat transfer. This selection process is complicated by the myriad of available shading products, often with variable geometries, and the inability of current evaluation and rating techniques, based on center-glass one-dimensional computer analysis, to accurately simulate shading systems. The result is that expensive and time-consuming calorimetric testing is the only alternative for assessing the thermal performance of shading systems.

Typically, the analysis of the center-glass area of glazing systems takes advantage of the fact that there is no appreciable overlap between the band of solar wavelengths (0.3 to 3 μm) and the band of longer wavelengths (3 to 50 μm) by which radiant transfer occurs. This absence of overlap between the solar and longwave spectra allows the analysis to be carried out in two steps. First, a solar-optical calculation determines how much solar radiation is absorbed at each layer and how much is transmitted to the indoor space. Second, a heat transfer analysis is used to perform an energy balance at each layer in which the net heat transfer from a layer must equal the amount of absorbed solar radiation (e.g., Wright 1998). The simultaneous solution of the resulting set of energy balance equations yields the temperature of each glazing layer as well as the various values of heat flux and heat flux components at each location within the system.

In order to expand the scope of center-glass simulation, the front and back surfaces of the shading layer are assigned spatially averaged optical properties, called "effective" optical properties. The use of effective optical properties allows the shading layer to be treated as a homogeneous, planar layer that can be placed at any location within a glazing system (e.g., indoor side, between glazing layers). The entire glazing

Darryl S. Yahoda is senior technology specialist in the Market Knowledge Department, Union Gas Ltd., Toronto, Ontario, Canada. **John L. Wright** is head of the Advanced Glazing Systems Laboratory, associate professor and deputy chair in the Department of Mechanical Engineering, University of Waterloo, Waterloo, Ontario, Canada.

system can be treated as an n-node array consisting of n-3 glazing layers, one shading layer, plus the indoor space (node 1) and outdoor environment (node n) as shown in Figure 1 where the shading layer is included as the *i*th node.

A complete energy flow analysis requires the effective optical properties, both solar and longwave, of the shading layer. Methods for determining the longwave effective optical properties were dealt with in the first step of this study (Yahoda and Wright 2004). A number of models for solar radiation transport through venetian blinds exist in the literature. These models are briefly discussed in the following paragraphs.

Rheault and Bilgen (1989) describe a heat transfer analysis for an automated venetian blind window system where the blind is located between two glass panes. The model was used to simulate the thermal performance of the system to determine energy savings for summer and winter conditions. The solar radiation model considers a closed cavity that is bounded by the glass panes and two adjacent blind slats. The slat surfaces are divided in two, in proportions dependent on the incidence angle of the solar radiation. The assumption is made that all slat surfaces can be characterized using a total (i.e., spectrally averaged) diffuse solar reflectivity. Longwave radiation exchange between surfaces is determined using a conventional irradiance/radiosity model (e.g., Incropera and deWitt 1996), each surface having a known emissivity.

Parmelee and Aubele (1952) developed a solar transport model through slat-type shading as a research project for The American Society of Heating and Ventilating Engineers (ASHVE). The research describes equations for the determination of the absorbing, reflecting, and transmitting characteristics of slat-type shades for solar radiation (beam and diffuse). Each effective optical characteristic of the shade is dependent on the solar reflectance of the slat material, the profile angle, and the geometry of the slat assembly. The research is based on treating optical characteristics of the slat surfaces as either specular or diffuse. From the blind geometry, the fractions of the incident beam radiation that will undergo a given number of specular reflections are determined. The effective optical properties for the blind can be determined by considering the amount of beam radiation absorbed and reflected at each specular reflection. For slat surfaces whose optical characteristics are modeled as being perfectly diffuse, the slat that is directly illuminated by beam radiation can be split into illuminated and a shaded elements. The view factors between the openings, the two elements, and the adjacent surface that is completely shaded from beam radiation can be computed. The effective optical properties for the blind can be determined by considering the beam radiation that is transmitted directly in addition to the transmission and reflection that occurs through the diffuse reflections of the slat surfaces. The model also gives a treatment for diffuse solar radiation. The sky is treated as a quarter sphere and divided into 81 "patches." The diffuse transmittance is determined by dividing the sum of the radiant energy transmitted through the shade by the sum of the radiant energy from the patches incident on the shade.

The WIS (Advanced Window Information System) program (Rosenfeld et al. 2000) contains a model for calculations involving horizontal and vertical blind systems. The shaded fenestration system is modeled using multiple layers. The blind is represented as a layer with effective optical properties, which are based on the optical properties of the slat surfaces, the blind geometry (slat width, slat spacing, slat angle), and the angle of incidence of the beam solar radiation. The beam radiation that is transmitted or reflected by the blind is split in two parts—an undisturbed part and a disturbed part. The undisturbed part is transmitted as beam radiation by the blind directly without interacting with slat surfaces. The disturbed part interacts with the slat surfaces, which are assumed to be anisotropic diffuse reflectors only (no specular reflections). Each slat is divided into five equal elements with negligible improvement observed in considering more elements (ISO 2002). The effective properties are determined by considering two adjacent slats, with the front and back openings modeled as perfectly transparent surfaces. The model is described as follows (Rosenfeld et al. 2000):

> Firstly, the matrix of view factors is determined between each of the 10 segments mutually and with the surfaces 1 and 2. Secondly, multiple reflections at the segments are taken into account by converting the view factor matrix into the configuration matrix using the reflectance of the lamellae. The process is carried out at each required wavelength (Rosenfeld et al. 2000).

More detail is found in the ISO DIS standard (ISO 2002).

The Rosenfeld Simple Model (Rosenfeld et al. 2000) is based on a multi-layer representation of a complex glazing. This model was developed with the restriction that all solar radiation is normally incident. From the blind geometry, the fractions of the incident beam radiation that will undergo *n* specular reflections are determined. The beam radiation that is reflected diffusely is modeled as behaving in a quasi-specular

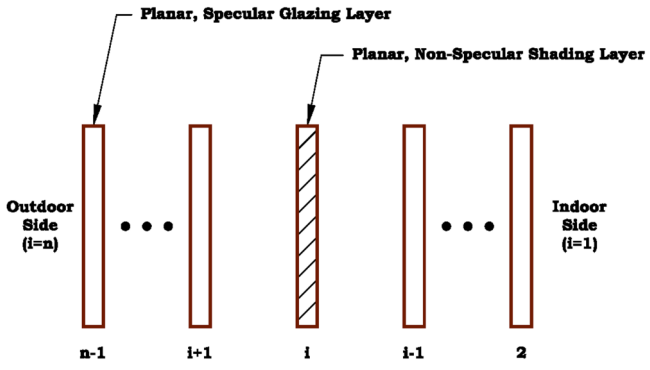

Figure 1 *Layer representation of glazing system with venetian blind.*

fashion. For light undergoing two or more reflections on its way through the blind, at each subsequent reflection a fraction F of the diffusely reflected light is assumed to proceed through the blind in the same way as the specular component. The fraction $(1–F)$ is reflected backward and retraces the path of specular reflection, with portions being absorbed at each reflection, before emerging from the illuminated side (Rosenfeld et al. 2001). The model uses the adjustable parameter F to describe how closely the diffuse reflections are concentrated at angles near the specular direction. The fraction of light reflected and absorbed at each reflection can be determined to yield the effective transmittance, reflectance, and absorptance of the blind. More detail is found in Rosenfeld et al. (2001). The performance of the Simple Model in predicting the total solar energy transmittance was compared with the WIS model and experimental measurements (Rosenfeld et al. 2000). The Simple Model is in good agreement with the experimental measurements up to slat angles of 60° while the WIS model underestimates the measured solar transmittance, in part, because of the assumption of "Lambertian distribution for reflection at the blind" (Rosenfeld et al. 2000). It should also be noted that in the WIS/Simple Model comparisons, different values of slat reflectance were used for each model. The magnitude of the slat reflectance used is not reported for either model.

Pfrommer et al. (1996) devised a model that divides solar radiation transmission through slat-type blinds into four different paths: (1) the unshaded transmission of the direct beam (direct transmittance); (2) the directly reflected beam from the slat surfaces (directly reflected transmittance), which may be pure diffuse, pure specular, or any combination; (3) the unshaded transmission of diffuse radiation (diffuse transmittance); and (4) the reflected diffuse radiation at the slat surfaces (diffuse-reflected transmittance). The direct transmittance is calculated from the blind geometry and the projected sun height-angle (profile angle). The directly reflected transmittance consists of two parts: a direct-to-diffuse reflected radiation portion and a specular-reflected radiation portion, which are related by the shining factor s of the slat material. The shining factor becomes 1 for diffuse reflection or 0 for specular reflection. The direct-to-diffuse reflected radiation is calculated by considering multi-reflections up to the second reflection. This simplification was found to cause errors of less than 5% for light slats (slat reflectance = 0.6) and less than 1% for dark slats (slat reflectance = 0.2). Similarly to the Parmelee and Aubele (1952) model for diffuse slats, the view factors between the illuminated slat area and the indoor space, the illuminated slat area and the upper slat, and the upper slat and the indoor space are determined. The direct-to-diffuse reflected radiation is computed from the view factors and the slat material reflectance. The model, as described, restricts the top and bottom slat surfaces to have the same reflectance. The specular-reflected portion of the direct transmittance is modeled using a rigorous analytical solution with no approximations. As with the Parmelee and Aubele (1952) model and the Simple Model of Rosenfeld et al. (2000), the effective optical properties can be determined by considering the amount of beam radiation absorbed and reflected at each specular reflection. The diffuse transmittance is based on the assumption of an isotropic sky. Cutoff angles, which give an angular representation of the open space between the slats, are determined from the blind geometry. The diffuse transmittance is found by integrating the transmitted radiation from each slice of the sky (or ground) across the vault between the cutoff angles and dividing it by the total radiation from the sky (or ground). The diffuse-reflected transmittance uses an analytical solution, which requires the assumption that the slat surfaces are purely diffuse.

Pfrommer et al. (1996) investigated the effects of modelling the slats as being flat and found that the influence of slat curvature decreases as the radius of curvature increases. For normal blind geometries (slat width ~ slat spacing), the influence was negligible. However, for highly curved slats (slat radius of curvature < slat width), the influence of the slat curve may be important.

Other models for predicting the solar heat gain of glazing systems are found in the literature. Farber et al. (1963, 1964) incorporated the Parmelee and Aubele (1952) model into a model for predicting the solar heat gain of a double glazing with a venetian blind. McCluney and Mills (1993) developed an expression for modifying the shading coefficient to include the effects of interior shading using a simplified model. The model is based on the restrictive assumptions that sunlight is always at normal incidence to the glazing, the shading layer is specularly reflecting, and the shade will have no effect on the inward-flowing fraction of the glazing layer. In spite of the restrictive assumptions, predicted shading coefficient values agreed well with the measured values of McCluney and Mills (1993). The references listed immediately above are not directly concerned with modeling shading elements as layers with effective optical properties and, therefore, are not discussed in detail.

OBJECTIVES

The purpose of the current work is to develop methods for determining the effective solar-optical properties of the shading layer, which can be used in solar-optical analysis of the glazing system. The research discussed in the proceeding sections describes methods for calculating the effective solar-optical properties of shading elements with arrangements of slats such as a venetian blind. The models presented in this research overcome some of the limitations of the previous models by removing restrictions on values of the profile angle, allowing for different properties for each slat surface (top and bottom), and treatment of the slat surfaces as having both diffuse and specular components of reflection in the solar spectrum. Comparisons between results obtained from this research and those presented in the literature are also made.

The effective solar-optical property models described in this paper are based on fundamental radiative analysis and

straightforward geometrical analysis. The resultant effective solar-optical properties are functions of the solar geometry (i.e., the direction from which beam solar radiation is incident), the reflectivity of the slat material, and the blind geometry, which is composed of the tilt angle of the slats (slat angle), ϕ; slat width, *w*; and the spacing between adjacent slats, *s*.

Methods have also been devised for integration of the "beam incidence" effective solar properties in order to determine the corresponding properties that apply to diffuse insolation, but are not reported here.

EFFECTIVE SOLAR-OPTICAL PROPERTIES

The effective solar-optical properties of the shading layer are determined by examining an area of the layer that will be representative of the layer as a whole. For a venetian blind, the optical characteristics of the area between two adjacent slats are representative of the entire layer. The two adjacent slat surfaces of width, *w*, with fictitious surfaces at the front and back openings equal in length to the slat spacing, *s*, constitute an enclosure as shown in Figure 2. Note that Figure 2 also shows the slat angle, ϕ.

Solar-Beam Radiation

Solar-beam radiation incident on a shading layer surface can be modeled as being transmitted or reflected by the shading layer through the following five paths:

1. transmitted without encountering the slat surfaces,
2. transmitted through the shading layer by means of only specular reflections at the slat surfaces,
3. transmitted through the shading layer after one or more diffuse reflections at the slat surfaces,
4. reflected from the shading layer by means of only specular reflection at the slat surfaces,
5. reflected from the shading layer after one or more diffuse reflections at the slat surfaces.

These five paths for transmission and reflection of solar beam radiation are depicted in Figure 3. The paths where the incident solar beam radiation leaves the front or back of the blind enclosure (reflection or transmission, respectively) as beam radiation will be treated together and called "beam-to-beam" cases. The effective beam-to-beam solar-optical properties will be given the subscript *bb*. The cases where the incident beam radiation leaves the front or back of the blind enclosure as diffuse radiation will be treated separately and called "beam-to-diffuse" cases. The effective beam-to-diffuse solar-optical properties will be given the subscript *bd*.

Properties of the Slat Surface and the Beam/Diffuse Split

When beam radiation is incident on an opaque blind slat surface, a portion of the beam, ρ_{beam}, will be reflected and the remainder will be absorbed. To incorporate the directional and

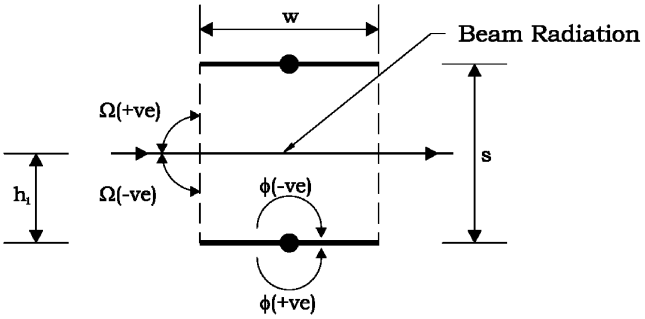

Figure 2 *Blind enclosure conventions for beam-to-beam calculations.*

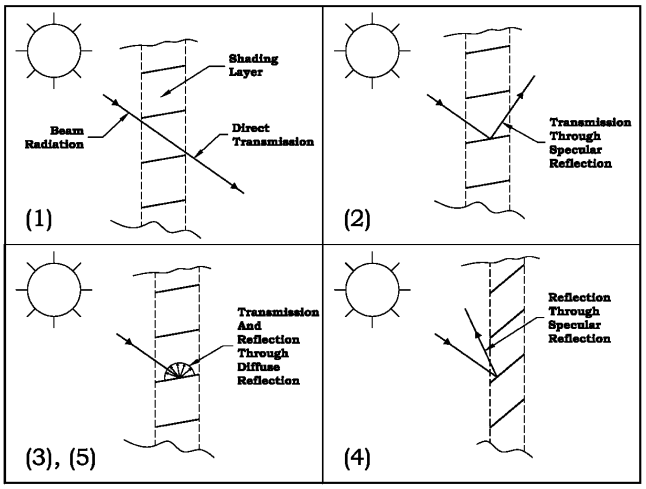

Figure 3 *Paths for transmission and reflection of beam radiation.*

spectral dependence of a slat material's reflectance into the beam radiation model requires detailed optical property data for each specific slat material. Such optical property data are not readily available. To overcome this problem ρ_{beam} is assumed to be directionally and spectrally independent, i.e., a constant. This assumption is common in other models found in the literature, with the hemispherical reflectance measured at normal incidence generally used as ρ_{beam} (Rosenfeld et al. 2000).

The assumption regarding directional independence simplifies the solar analysis substantially. If desired, the model presented in subsequent sections can readily be extended to include spectral characteristics, but it is unlikely for slat materials to be spectrally selective.

Models described in the literature also entail the assumption that the slat surface will reflect beam radiation, either specularly or diffusely, as shown in Figure 4a and Figure 4b, respectively.

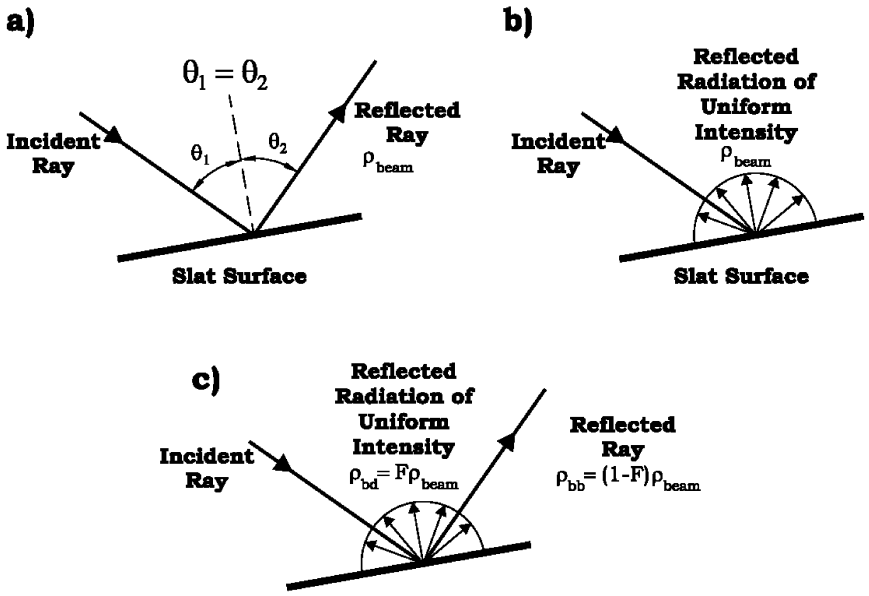

Figure 4 *Reflection at the slat surface: (a) specular, (b) diffuse, (c) specular and diffuse.*

In fact, slat materials will reflect a portion of the beam radiation specularly and the remainder diffusely (Parmelee and Aubele 1952). In this work the slat surface is modeled as shown in Figure 4c. Specifically, the analysis makes use of beam-to-beam reflectivity, ρ_{bb}, and the beam-to-diffuse reflectivity, ρ_{bd}, of the blind slat material. ρ_{bb} and ρ_{bd} are the fractions of beam radiation incident at the slat surface, reflected specularly, and reflected diffusely, respectively. These two optical properties are related using the concept of the beam/diffuse split, F, which is a measure of how specularly or diffusely the slat material reflects beam radiation. F is also referred to in the literature as the shining factor, σ, of the material (Pfrommer et al. 1996). For purely specular behavior F = 0 and for purely diffuse behavior F = 1. F is also assumed to be constant, regardless of the direction or wavelength of the incident beam radiation. ρ_{bb} and ρ_{bd}, can be expressed in terms of the slat material's beam reflectivity, ρ_{beam}, and the beam/diffuse split, F, as follows:

$$\rho_{m,bb} = (1 - F_m)\rho_{m,beam} \quad (1)$$

$$\rho_{m,bd} = F_m\rho_{m,beam} \quad (2)$$

where the subscript m is used to specify whether the top slat surface (m = top) or the bottom slat surface (m = bottom) is being described.

Measurements by Parmelee et al. (1953) and Rosenfeld et al. (2001) show that approximately 10% of the reflected beam is reflected specularly and 90% diffusely, suggesting that F = 0.9 for slat materials.

In addition, the diffuse-to-diffuse reflectivity, ρ_{dd}, which is the fraction of incident diffuse solar radiation that is reflected at the slat surface, is needed to complete the analysis. The assumption that the slat beam reflectivity, ρ_{beam}, is not directionally dependent means that $\rho_{dd} = \rho_{beam}$ for consistency because the diffuse radiation is essentially beam radiation of equal intensity coming from all directions. Thus,

$$\rho_{m,dd} = \rho_{m,beam}. \quad (3)$$

Profile Angle and Solar Geometry

The ability of a slat-type shading device to intercept incoming beam radiation is not only dependent on the geometry of the shading device but also on the profile angle, Ω, of the incident beam radiation. The profile angle is the projected solar altitude angle and is defined as the angle between the normal to a surface and the projection of the sun's rays on a plane normal to the same surface (Kreith and Kreider 1978). The profile angle for solar beam radiation is shown in Figure 5.

The profile angle can be determined from the wall-solar azimuth, γ, and the solar-altitude, β, as follows:

$$\Omega = \tan^{-1}\left(\frac{\tan\beta}{\cos\gamma}\right) \quad (4)$$

The solar-altitude, β, and wall-solar azimuth can be determined from the fundamental angles of solar geometry. Relations regarding the fundamental solar angles can be found in many references, including the *ASHRAE Handbook—Fundamentals* (ASHRAE 2001).

Beam-to-Beam Calculations

The fractions of incident beam radiation that will be transmitted and reflected as beam radiation can be determined by considering the geometry of the system (w, s, and ϕ) and the

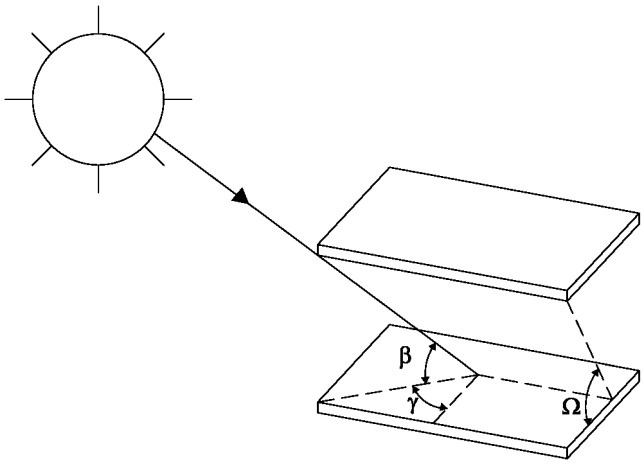

Figure 5 *Profile angle, Ω, for solar beam radiation (illustrated with horizontal slats, ϕ = 0).*

profile angle of the incident beam radiation, Ω. Since all beam-to-beam reflections are, by definition, specular, the path of each ray through the blind enclosure for each specific geometry and profile angle will be fixed by its entry point at the surface of the shading layer. This entry point is characterized by a ray "entrance height," h_1, as shown in Figure 2, which is defined as the distance from the tip of the lower slat to the ray's point of entry at the shading layer surface. An entrance height algorithm was developed to determine entrance height ranges that describe the beam radiation behavior through the shading layer.

Entrance Height Algorithm

The entrance height algorithm is based on the system geometry (w, s, and ϕ) and the profile angle of the incident beam radiation, Ω. Several cases were examined separately because of the changing behavior of the system with different combinations of w, s, ϕ, and Ω. Figure 2 defines the geometric conventions used in the algorithm. The entrance height algorithm is used to define height ranges through which rays will undergo a given number of reflections before emerging from the enclosure. The ray entrance heights are described using the general notation, $h_{1,n,Z}$, where the additional subscript n signifies the number of reflections the ray undergoes before leaving the enclosure and Z signifies whether the entrance height is an upper limit, *UL*, or lower limit, *LL*. Comprehensive details of the derivation of the entrance height algorithm can be found in (Yahoda 2002).

The entrance height algorithm was developed from two sets of cases. The first set, Case Set 1, treats situations where the slat angle, ϕ, and the profile angle, Ω, are of the same sense, both either positive or negative. The second set of cases, Case Set 2, treats situations where ϕ and Ω are of the opposite sense. Table 1 and Table 2 list the geometries of cases that compose each case set.

Table 1. Case Set 1—Entrance Height Algorithm (ϕ, Ω of same sign)

Case	Geometry (ϕ, Ω of same sign)
1	$2\lvert\phi\rvert + \lvert\Omega\rvert < 90°$
2	$2\lvert\phi\rvert + \lvert\Omega\rvert \geq 90°$, $\lvert\phi\rvert + \lvert\Omega\rvert < 90°$
3	$\lvert\phi\rvert + \lvert\Omega\rvert \geq 90°$, $w \geq s$, $\lvert\Omega\rvert < 90°$
4	$\lvert\phi\rvert + \lvert\Omega\rvert \geq 90°$, $w < s$, $\lvert\Omega\rvert < 90°$
5	$\lvert\Omega\rvert \geq 90°$

Table 2. Case Set 2—Entrance Height Algorithm (ϕ, Ω of same sign)

Case	Geometry (ϕ, Ω of same sign)
6	$2\lvert\phi\rvert - \lvert\Omega\rvert < 90°$, $\lvert\Omega\rvert \geq \lvert\phi\rvert$, $\lvert\Omega\rvert < 90°$
7	$2\lvert\phi\rvert - \lvert\Omega\rvert < 90°$, $\lvert\Omega\rvert < \lvert\phi\rvert$, $\lvert\Omega\rvert < 90°$
8	$2\lvert\phi\rvert - \lvert\Omega\rvert \geq 90°$, $\lvert\Omega\rvert < 90°$
5	$\lvert\Omega\rvert \geq 90°$

Table 3. Coefficient Values for Entrance Height Equations

Case	A	B	C	D
1	1	1	1	n/a
2	n/a	n/a	n/a	1
6	–1	1	–1	n/a
7	1	–1	–1	n/a
8	n/a	n/a	n/a	–1

Cases 1, 6, 7

Equations 5-8 are general expressions for the upper and lower ray entrance heights for geometry that is characterized by Cases 1, 6, and 7. The values of the coefficients A, B, and C are listed in Table 3 for each case and for each case if there is direct transmission $h_{1,0,UL} = s$.

For even numbers of reflections,

$$h_{1,n(even),UL} = \frac{w\sin(A|\phi| + B|\Omega|) - \left(\frac{n}{2}\right)s\cos(2|\phi| + C|\Omega|)}{\cos|\Omega|} - \left(\frac{n}{2} - 1\right)s, \quad (5)$$

where $n = 2, 4, \ldots, n(\text{even})$,

$$h_{1,n(even),LL} = \frac{w\sin(A|\phi| + B|\Omega|) - \left(\frac{n}{2}\right)s\cos(2|\phi| + C|\Omega|)}{\cos|\Omega|} - \left(\frac{n}{2}\right)s, \quad (6)$$

where $n = 0, 2, \ldots, n(\text{even})$, and for odd numbers of reflections,

$$h_{1,n(odd),UL} = \frac{w\sin(A|\phi| + B|\Omega|) - \left(\frac{n-1}{2}\right)s\cos(2|\phi| + C|\Omega|)}{\cos|\Omega|} - \left(\frac{n-1}{2}\right)s, \quad (7)$$

where $n = 1, 3, \ldots, n(\text{odd})$,

$$h_{1,n(odd),LL} = \frac{w\sin(A|\phi| + B|\Omega|) - \left(\frac{n+1}{2}\right)s\cos(2|\phi| + C|\Omega|)}{\cos|\Omega|} - \left(\frac{n-1}{2}\right)s, \quad (8)$$

where $n = 1, 3, \ldots, n(\text{odd})$.

Cases 2 and 8

Equations 9 and 10 are general expressions for the upper and lower ray entrance height ranges for geometry that is characterized by Cases 2 and 8. The values of the coefficient D are listed in Table 3 for each case and if there is direct transmission $h_{1,0,UL} = s$. For these two cases, transmission through the shading layer is possible only through even numbered reflections and, thus,

$$h_{1,n(even),UL} = \frac{w\sin(|\phi| + D|\Omega|) - (n-2)s\cos(|\phi| + D|\Omega|)}{\cos|\Omega|}, \quad (9)$$

where $n = 2, 4, \ldots, n(\text{even})$;

$$h_{1,n(even),LL} = \frac{w\sin(|\phi| + D|\Omega|) - ns\cos|\phi|\cos(|\phi| + D|\Omega|)}{\cos|\Omega|}, \quad (10)$$

where $n = 0, 4, \ldots, n(\text{even})$.

For the geometry represented in these two cases, rays can also be back-reflected (i.e., reflected back through the enclosure entrance). To determine whether or not any rays will be reflected out the enclosure entrance, the critical ray entrance height, $h_{1,c}$, which is the upper limit on the ray entrance height for back reflections out the enclosure entrance, can be determined as follows:

$$h_{1,c} = \frac{-s\cos(2|\phi| + D|\Omega|)}{\cos|\Omega|} \quad (11)$$

If $h_{1,c}$ is between zero and s, any rays entering the enclosure below $h_{1,c}$ will be back-reflected through the enclosure entrance after one reflection.

Case 3

All rays entering the blind enclosure will be reflected out the enclosure entrance after one reflection.

Case 4

Since $w < s$, there is a possibility that some rays will be directly transmitted before contacting the slat surface. The lower limit on the ray entrance height for direct transmission, $h_{1,0,LL}$, can be determined as follows:

Table 4. Validation of Upper and Lower Entrance Heights

IF	$h_{1,n,UL}$	$h_{1,n,LL}$
$h_{1,n,UL} \geq s$ and $h_{1,n,LL} \geq s$	0	0
$h_{1,n,UL} \geq s$ and $0 \leq h_{1,n,LL} < s$	s	$h_{1,n,LL}$
$h_{1,n,UL} \geq s$ and $h_{1,n,LL} < 0$	s	0
$0 \leq h_{1,n,UL} \leq s$ and $h_{1,n,LL} \geq 0$	$h_{1,n,UL}$	$h_{1,n,LL}$
$0 \leq h_{1,n,UL} \leq s$ and $h_{1,n,LL} < 0$	$h_{1,n,UL}$	0
$h_{1,n,UL} < 0$	0	0

$$h_{1,0,LL} = \frac{w\sin(|\phi| + |\Omega|)}{\cos|\Omega|} \quad (12)$$

If $h_{1,0,LL} > s$, no rays will be directly transmitted. If $h_{1,0,LL} \leq s$, any ray entering the blind enclosure from this height or higher will be directly transmitted. The entrance height upper limit, $h_{1,0,UL}$, will be equal to the slat spacing, s. Any rays entering the enclosure from a height lower than $h_{1,0,LL}$ will be back-reflected through the enclosure entrance after the first reflection at the slat surface.

Case 5

When $\Omega \geq 90°$, beam radiation will not interact with the blind enclosure.

Fractions for Transmission Through n-Reflections

Using the appropriate set of equations, stated previously, for given values of ϕ, Ω, s, and w, the upper and lower limits on the ray entrance heights for transmission through n reflections can be calculated. Before the fractions for transmission through n reflections can be determined, the validity of the upper and lower heights must be checked. Table 4 summarizes the validation logic for the entrance heights. The first column describes the situation the calculated entrance heights fall under. The second and third columns are the values that must be assigned to the upper and lower limit entrance heights before the fractions for transmission through n-reflections are calculated.

The fraction of incident rays that will undergo transmission through n reflections, P_n, is given by the fraction of the aperture area that accepts radiation that will undergo n reflections while in the process of transmission. Therefore,

$$P_n = \frac{h_{1,n,UL} - h_{1,n,LL}}{s}, \quad (13)$$

where $n = 0, 1, \ldots, n$.

The equations presented in the previous section can be coded to efficiently predict the fraction of incident rays that will undergo transmission through n reflections for given values of ϕ, Ω, s, and w. A similar method for estimating beam-

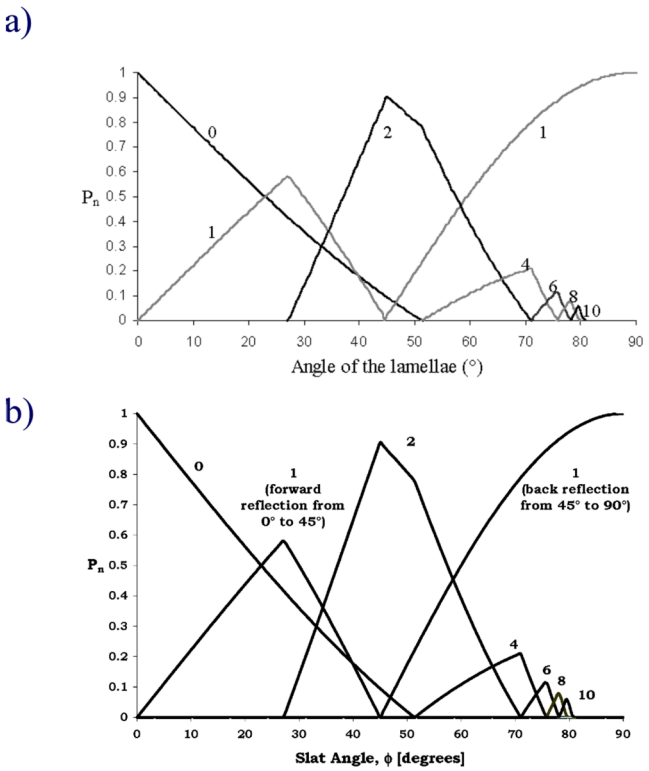

Figure 6 *P_n vs. slat angle for normal incidence: (a) Rosenfeld et al. (2001) Simple Model, (b) Yahoda-Wright (2004) Model.*

to-beam transmission through *n* reflections was developed by Rosenfeld et al. (2001) but is restricted to normal incidence only. Figure 6a is a plot from Rosenfeld et al. (2001) of P_n as a function of slat angle for w = 16 mm and s = 12.5 mm. To preserve clarity in the figure, only fractions up to the 10th reflection are shown. Figure 6b is a plot of P_n as function of slat angle under the same conditions used by Rosenfeld et al. and calculated with Equation 13 and the entrance height equations presented earlier. The two figures are essentially identical. The behavior of P_n in Figure 6 can be explained in terms of the case geometry summarized in the previous section. For slat angles from 0° to 45°, the geometry is Case 1, where transmission through even and odd reflections is possible. Direct transmission and transmission through one and two reflections is observed. When the slat angle reaches 45°, the geometry falls under Case 2, where transmission can occur only through even numbered reflections, with back reflection also being possible.

Using the same blind geometry as Figure 6, Figure 7 shows P_n as a function of slat angle for a profile angle of 45°. Note that changing the profile angle from 0° to 45° shifts the peak of the direct transmission curve from a slat angle of 0° to –45°, the slat angle where the beam radiation will be parallel

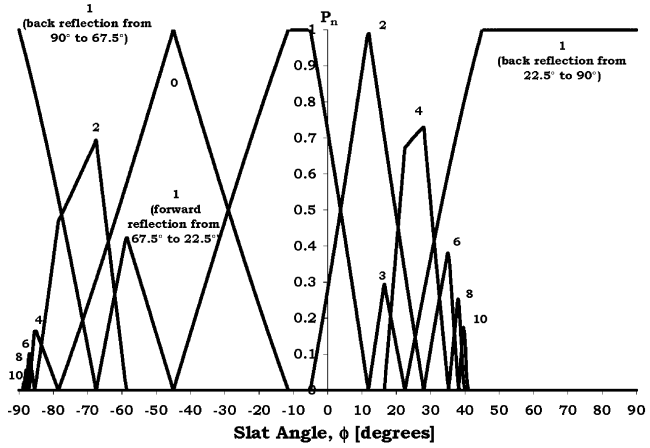

Figure 7 *P_n vs. slat angle for ϕ = 45° (Yahoda 2002).*

to the blind slats. Also of note is for $\phi \le -67.5°$ and $\phi \ge 22.5°$, all rays undergoing only one reflection are back-reflected through the enclosure entrance. This is expected because these cases of geometry fall under Case 2 and Case 8.

Effective Beam-to-Beam Solar-Optical Properties

The effective beam-to-beam solar-optical properties can be determined from the fractions for transmission through *n* reflections (Equation 13) and the slat material's solar-optical properties. The effective beam-to-beam transmittance will be equal to the sum of the beam radiation that is transmitted through the shading layer directly (without interacting with the slat surfaces) and by specular reflections at the slat surfaces. After each reflection, the fraction of the initial amount of beam radiation incident on the next slat surface will be equal to the beam-to-beam reflectivity, ρ_{bb}, of the previous slat surface. Assigning the top surface (bottom of the slat) a beam-to-beam reflectivity, $\rho_{top,bb}$, and the bottom surface (top of the slat) a beam-to-beam reflectivity, $\rho_{bottom,bb}$, the effective properties can be calculated as follows:

$$\tau_{eff,bb} = \sum_{i=0}^{n(even)} P_i \rho_1^{\frac{i}{2}} \rho_2^{\frac{i}{2}} + \sum_{j=1}^{n(odd)} P_j \rho_1^{\frac{j+1}{2}} \rho_2^{\frac{j-1}{2}} \qquad (14)$$

where i = 0, 2, 4,..., n (even) and j = 1, 3, 5,..., n(odd).

$$\rho_{eff,bb} = P_{1(back)} \rho_1 \qquad (15)$$

If the bottom slat surface intercepts the beam radiation first, $\rho_1 = \rho_{bottom,bb}$ and $\rho_2 = \rho_{top,bb}$. If the top surface intercepts the beam radiation first, $\rho_1 = \rho_{top,bb}$ and $\rho_2 = \rho_{bottom,bb}$.

It is important to note that P_1 will contribute to the effective transmittance if the values of ϕ and Ω correspond to Case 1, 6, 7 geometry. Otherwise, P_1 corresponds to back-reflection and will contribute to the effective reflectance.

Beam-to-Diffuse Calculations

The diffuse radiation examined in this section originates from diffusely reflected beam radiation. Since different portions of both the top and bottom slat surfaces intercept beam radiation, which will have undergone different numbers of reflections, it is not reasonable to treat the slats as being uniformly irradiated. The amount of incident beam radiation that will be transmitted or reflected as diffuse radiation is determined by considering the geometry of the system (w, s, and ϕ) and the profile angle of the incident beam radiation, Ω. All reflected diffuse radiation is assumed to remain diffuse. The following section describes how the slats can be separated into shaded and illuminated areas.

Slat Separation and Illumination Assignment

There are many options available to separate the slats into different areas. Van Dijk (ISO 2002) suggests that each slat should be divided into five equal elements, with additional elements providing negligible improvement. Parmelee and Aubele (1952) and Pfrommer et al. (1996) consider only diffuse radiation resulting from directly intercepted beam radiation. This approach involves dividing the directly illuminated slat into illuminated and shaded portions while the other slat is left undivided. The approach described in this section goes one step further in that the slats are subdivided on the basis of where each slat intercepts beam radiation, either directly or through one-reflection. Using this approach, both slats potentially have some degree of beam illumination.

The progress of beam radiation through many specular reflections can readily be tracked. However, diffuse radiation leaving a slat surface, whose source is beam radiation incident on that surface, is tracked only up to and including the second surface encountered by the beam radiation. Justification for this approach is offered by considering the extreme cases. If the slats are of high specular reflection, most of the radiation will be transmitted or reflected out of the shading layer as beam radiation and the diffuse component will be relatively unimportant, especially after the second specular reflection. If the slats are of high diffuse reflection, most of the beam radiation will be converted to diffuse radiation by the second specular reflection, leaving only a small amount of beam radiation to be reflected diffusely on the third reflection. If the slats are highly absorptive, most of the beam radiation will be absorbed, leaving only negligible amounts of beam radiation to be reflected diffusely or specularly on the third reflection. On the basis of this qualitative argument, only diffuse radiation resulting from the reflection of beam radiation up to and including the second reflection was included. (Part of the diffuse radiation neglected at subsequent specular reflections will be missing from the beam-to-diffuse transmittance and reflectance of the shading layer and thus will manifest itself as a small increase in the effective absortance of the shading layer.) This simplification permits the blind enclosure to be treated generally as an eight-surface enclosure. Each surface is labeled as shown in Figure 8.

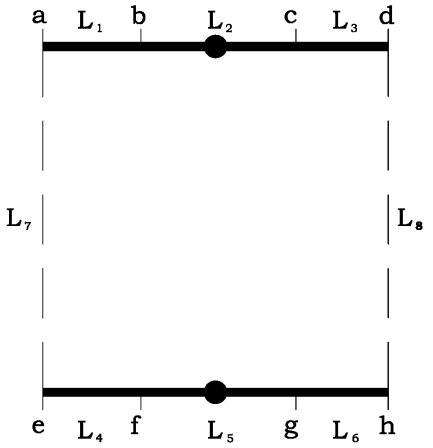

Figure 8 *Blind enclosure dimensions for beam-to-diffuse calculations.*

The top and bottom slats are split into three surfaces each, labelled L_1, L_2, L_3 and L_4, L_5, L_6, respectively. Although the enclosure is represented generically by eight surfaces, depending on the blind geometry and profile angle, a minimum of four surfaces and a maximum of seven surfaces are actually needed.

Each slat can be divided into the correct number of surfaces by examining the beam radiation behavior for each specific case of profile angle and blind geometry. The path of the beam radiation that enters the top and the bottom of the enclosure entrance (at the slat tips) can be traced. The lengths along the bottom and top slats that a ray of beam radiation entering at the slat tip of the bottom of the entrance to the enclosure will travel, either directly or through one reflection, will be referred to as X_{1a} and X_{2a}, respectively. The lengths along the bottom and top slat that a ray of beam radiation entering at the slat tip of the top of the entrance to the enclosure will travel, either directly or through one reflection, will be referred to as X_{1b} and X_{2b}. Figure 9a is an example of how these lengths are defined.

Using Figure 9a as an example, beam radiation entering at the slat tip of the bottom of the entrance to the blind enclosure will strike the edge of the bottom slat, thus $X_{1a} = 0$. Assuming the slat reflection has some specular component, the same beam will reflect off the bottom slat and strike the top slat at a distance X_{2a} along the top slat. Beam radiation entering at the slat tip of the top of the blind enclosure will strike the bottom slat at a distance X_{1b} along the bottom slat. Again, assuming the slat reflection has some specular component, the same beam will reflect off the bottom slat and strike the top slat at a distance X_{2b} along the top slat.

From Figure 9a, the surface lengths for the eight-surface enclosure would be defined as shown in Figure 9b.

Referring to Figure 9b, for the top slat, $L_1 = X_{2a}$, $L_2 = X_{2b} - X_{2a}$, and $L_3 = w - X_{2b}$. For the bottom slat,

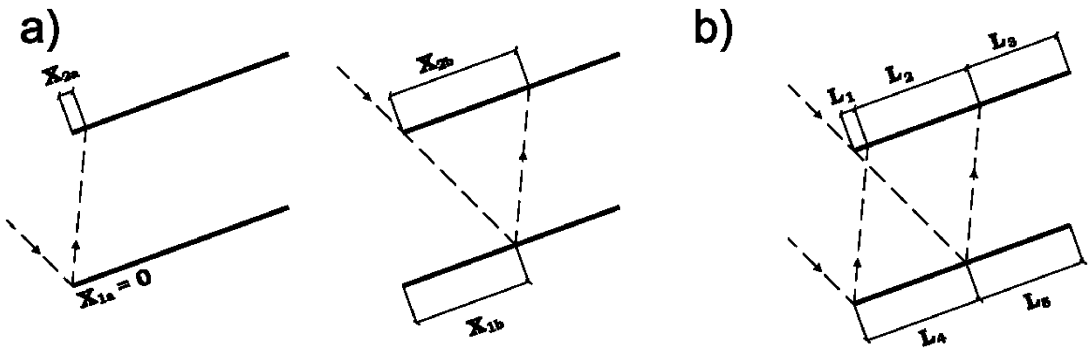

Figure 9 *(a) Example depicting X lengths, (b) example depicting surface lengths.*

$L_4 = X_{1b} - X_{1a}$, $L_5 = w - X_{1b}$, and $L_3 = 0$. In this case, seven surfaces are required in the beam-to-diffuse calculations. The surfaces represented by the lengths L_2 and L_4 are illuminated by beam radiation and the remaining surfaces are shaded from beam radiation.

The details for separating the bottom and top slats and assigning illuminated areas for all practical cases can be found in Yahoda (2002).

Enclosure View Factors

The view factors for the blind enclosure can be calculated after the slats have been separated into their respective surfaces and each surface has been assigned an illumination. To keep the view factor formulation general enough to treat all practical cases, the view factors for an eight-surface enclosure must be formulated based on the dimensions defined in Figure 8. The view factors can be calculated using Hottel's crossed-string method. The lengths for the eight-surface enclosure are determined in terms of w, s, ϕ, and the slat surfaces L_1 to L_6.

When a slat is separated into fewer than three surfaces, at least one surface of zero length will be present. Although the view factor between a surface of zero length to any other surface in the enclosure can mathematically be determined, it is not needed for subsequent radiant analysis and therefore does not need to be determined.

RADIANT ANALYSIS

The beam-to-diffuse calculations account for diffuse radiation that originates from beam radiation, which has been diffusely reflected from one of the slat surfaces. The diffuse radiation remains diffuse on successive reflections. With this in mind, the radiosity, J_i, of a surface is defined as the reflected portion of the diffuse radiation that originated from the other surfaces in the enclosure. Additionally, surfaces illuminated by direct or one-reflection beam radiation will have an additional radiosity component, which is the locally incident beam radiation that is reflected diffusely by the slat surface. This additional term will be treated as a diffuse "source" term and denoted S_i, where i is the surface number. The radiosity equations for this situation require knowledge of how the slat material reflects both beam and diffuse radiation diffusely, that is, the beam-to-diffuse and diffuse-to-diffuse reflectivities for both the top and bottom slats ($\rho_{top,bd}$, $\rho_{top,dd}$, $\rho_{bottom,bd}$, $\rho_{bottom,dd}$, respectively). The radiosity equations are simplified using the flat slat assumption, which means view factors between surfaces on the same slat will be zero.The radiosity equations are further simplified from the assumption that the two opening surfaces (L_7 and L_8) will transmit all incident radiation, resulting in $J_7 = 0$ and $J_8 = 0$. For the eight-surface blind enclosure, the radiosities of surfaces 1 to 6 are given by

$$J_i = \rho_{m,dd} G_i + S_i \,, \tag{16}$$

where m = top (for i = 1 to 3) or bottom (for i = 4 to 6) and the irradiance, G_i, of surfaces 1 to 8 is given by

$$G_i = \sum_{j=1}^{8} F_{ij} J_j \,. \tag{17}$$

Before Equations 16 and 17 can be applied, the so-called diffuse source terms, S_i, must be determined. The rate of beam solar radiation entering the blind enclosure is equal to the beam solar irradiance on the blind enclosure entrance, G_b, multiplied by the area of the opening A_7. The beam radiation available for the first reflection, off either the top or bottom slat surfaces, will be equal to the portion not directly transmitted by the blind enclosure. The beam radiation that is directly transmitted is $P_0 G_b A_7$; therefore, the beam radiation available for the first reflection will be $(1\text{-}P_0) G_b A_7$. Using the example shown in Figure 9b, surface 4 on the bottom slat receives unreflected beam radiation. The rate of energy leaving surface 4, $A_4 J_4$, is equal to sum of the rate of reflected diffuse radiation intercepted from the other surfaces and the rate of diffusely reflected beam radiation and, thus,

$$A_4 J_4 = \rho_{bottom,dd} G_4 A_4 + \rho_{bottom,bd} (1 - P_0) G_b A_7 \,. \tag{18}$$

Dividing both sides by A_4,

$$J_4 = \rho_{bottom,dd} G_4 + \rho_{bottom,bd} (1 - P_0) G_b \frac{A_7}{A_4} \,. \tag{19}$$

Table 5. Source Terms, S_i, for Radiosity Equations

	Illumination Assignment		
i	**Unreflected**	**1 Reflection**	**Shaded**
1, 2, 3	$\rho_{top,bd}(1-P_0)G_b\frac{A_7}{A_i}$	$\rho_{top,bd}\rho_{bottom,bb}(1-P_0-P_1)G_b\frac{A_7}{A_i}$	0
4, 5, 6	$\rho_{bottom,bd}(1-P_0)G_b\frac{A_7}{A_i}$	$\rho_{bottom,bd}\rho_{top,bb}(1-P_0-P_1)G_b\frac{A_7}{A_i}$	0

Comparing Equation 19 to Equation 16 shows that the source term for a surface that receives direct beam radiation will be of the form,

$$S_i: \rho_{bottom,bd}(1-P_0)G_b\frac{A_7}{A_4}.$$

After the first reflection there is a possibility that some of the beam radiation will leave the blind enclosure, either through reflection or transmission. This reduces the amount of beam radiation available for the next reflection. Again, referring to the example in Figure 8b, surface 4 on the bottom surface receives unreflected beam radiation. After the first reflection, beam radiation will leave the bottom surface at a rate of

$$\rho_{bottom,bb}(1-P_0)G_bA_7.$$

The rate of beam radiation that undergoes one reflection is

$$\rho_{bottom,bb}P_1G_bA_7.$$

Therefore, the rate of beam radiation available for the second reflection is

$$\rho_{bottom,bb}(1-P_0-P_1)G_bA_7.$$

Surface 2 on the top slat receives the one-reflection beam radiation. The rate of energy leaving surface 2 as diffuse radiation, A_2J_2, is equal to the sum of the rate of reflected diffuse radiation intercepted from the other surfaces and the rate of diffusely reflected beam radiation and, thus,

$$A_2J_2 = \rho_{top,dd}G_2A_2 + \rho_{top,bd}\rho_{bottom,bb}(1-P_0-P_1)G_bA_7. \quad (20)$$

Dividing both sides by A_2,

$$J_2 = \rho_{top,dd}G_2 + \rho_{top,bd}\rho_{bottom,bb}(1-P_0-P_1)G_b\frac{A_7}{A_2}. \quad (21)$$

Comparing Equation 21 to Equation 16 shows that the source term, S_i, for a surface receiving one-reflection beam radiation will be of the form,

$$S_i: \rho_{top,bd}\rho_{bottom,bb}(1-P_0-P_1)G_b\frac{A_7}{A_2}.$$

Table 5 lists the diffuse source terms for each surface and illumination assignment.

Using the appropriate diffuse source terms, the surface radiosities and irradiances can be determined. The irradiances of the openings to the blind enclosure, G_7 and G_8, constitute the portions of G_b that are reflected and transmitted, respectively. The effective beam-to-diffuse properties can be determined using the following:

$$\rho_{eff,bd} = \frac{G_7}{G_b} \quad (22)$$

$$\tau_{eff,bd} = \frac{G_8}{G_b} \quad (23)$$

The effective absorptance of the shading layer for beam radiation can be determined using the following:

$$\alpha_{eff,beam} = 1-\rho_{eff,bb}-\rho_{eff,bd}-\tau_{eff,bb}-\tau_{eff,bd} \quad (24)$$

Sensitivity to the Beam/Diffuse Split

A study was conducted to determine the sensitivity of the effective beam transmittance to the magnitude of the beam/diffuse split, F, for various values of w/s, ϕ, and ρ_{beam}. The effective beam-diffuse transmittance exhibited sensitivity to F only for cases with highly reflective slats ($\rho_{beam} = 0.8$), with the sensitivity present over the entire range of profile angles. This behavior is expected. Figure 10 illustrates the effect of the value of F for regular blind geometry ($w/s = 1$) and $\rho_{beam} = 0.8$ over the entire range of valid profile angles (-90° to 90°).

Model Comparisons

Parmelee and Aubele (1952) produced figures depicting the effective transmittance and absorptance for a shading layer with specular ($F = 0$) and diffuse ($F = 1$) slats at slat angles ϕ of 0°, 30°, and 45° for slat width-to-slat spacing ratios of 0.6 and 1.2 as a function of the slat material's absorptance ($1-\rho_{beam}$). Figures 11a and 12a, reproduced from Parmelee and Aubele (1952), are for $\phi = 45°$ and specular and diffuse slats, respectively. The beam radiation model described in this paper can be compared to the Parmelee figures by assigning the same absorptance to the top and bottom surfaces and by setting the beam/diffuse split parameter, F, to 0 for purely specular behavior and to 1 for purely diffuse behavior. Figures 11b and 12b were generated

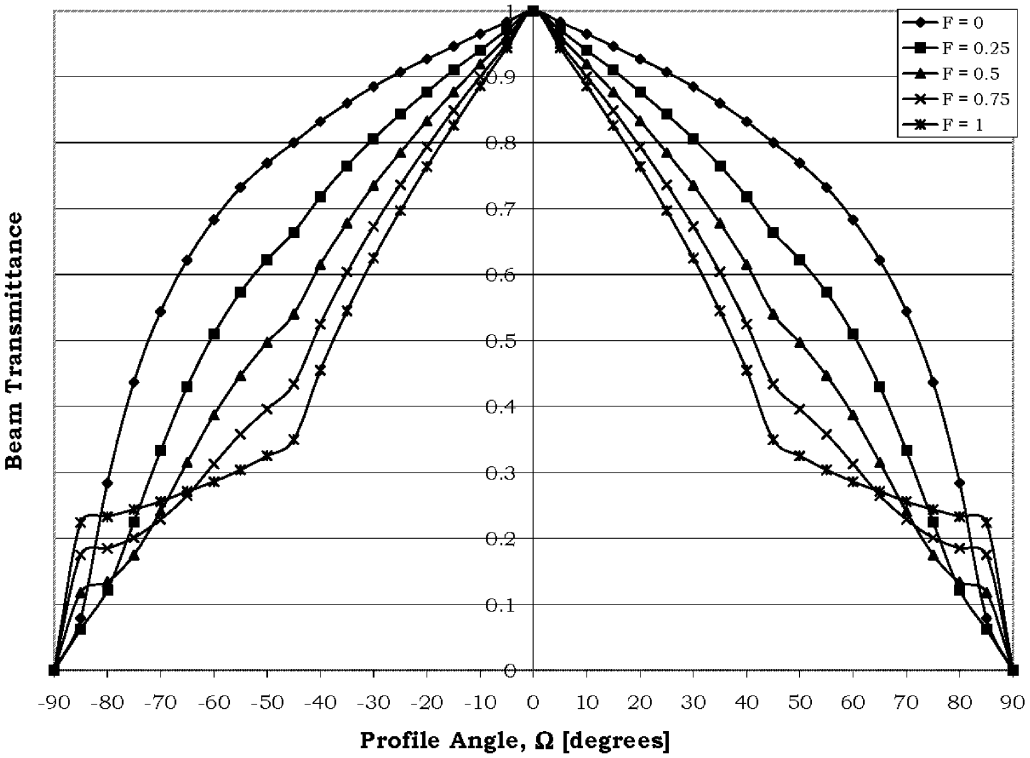

Figure 10 *Beam transmittance ($\tau_{eff,beam}$) vs. profile angle for various F (w/s = 1, ϕ = 0°, ρ_{beam} = 0.8).*

using the model described in this paper and compare very closely with the corresponding figures from Parmelee and Aubele (1952). This is expected because the Parmelee models for specular and diffuse slats are special cases of the models described above. These comparisons are of particular interest because Parmelee et al. (1953), in limited experimental testing, found good agreement between predicted and measured solar transmittance, absorptance, and reflectance for different shade (diffuse and specular slats) and glazing combinations (Parmelee et al. 1953).

CONCLUSIONS

A model has been developed for the calculation of the effective solar-optical properties of a venetian blind. These effective solar properties can be determined with respect to beam solar radiation incident from any direction. The same model can be incorporated to evaluate the corresponding properties with respect to diffuse insolation. The effective solar-optical properties can conveniently be used in a center-glass heat transfer analysis of a glazing system with a venetian blind, where the venetian blind is treated as a shading layer inserted anywhere in a series of glazing layers.

Beam solar radiation incident on the surface of a shading layer was modeled as transmitted or reflected through the following five paths: transmitted without encountering the slat surfaces (direct transmission), transmitted through specular reflections off the slat surfaces, transmitted through diffuse reflections off the slat surfaces, reflected through specular reflection off the slat surface, or reflected through diffuse reflections off the slat surfaces. The beam-to-beam model tracks specular reflections at the slat surfaces to determine the effective beam-to-beam reflectance and transmittance. The beam-to-diffuse model tracks diffuse reflections at the slat surfaces to determine the effective beam-to-diffuse reflectance and transmittance. The effective solar-beam absorptance is determined from the beam-to-beam and beam-to-diffuse reflectances and transmittances. Comparisons with results obtained by Parmelee and Aubele (1952) and Rosenfeld et al. (2000) showed the models were in good agreement.

Although comparisons with other, more restrictive models produced favorable results, extensive experimental validation of these models and integration into a glazing analysis are still required.

ACKNOWLEDGMENTS

This research was supported by Natural Sciences and Engineering Research Council (Canada).

REFERENCES

ASHRAE. 2001. *2001 ASHRAE Handbook—Fundamentals*, SI edition. Atlanta: American Society of Heating, Refrigerating and Air-Conditioning Engineers, Inc.

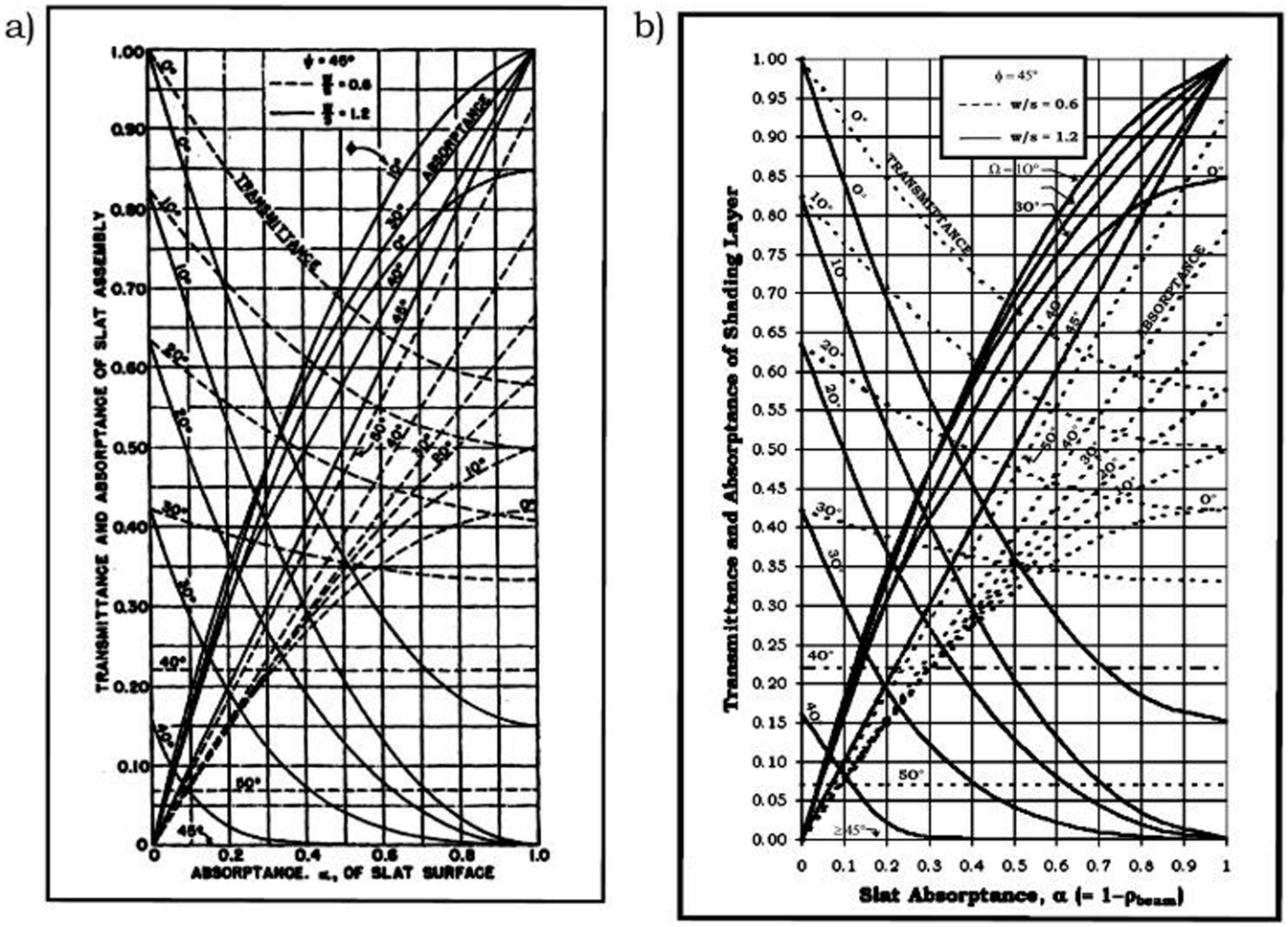

Figure 11 *Transmittance and absorptance of specular reflecting slats for monochromatic radiation, ϕ = 45°: (a) Parmelee and Aubele (1952)model, (b) Yahoda and Wright (2004) model.*

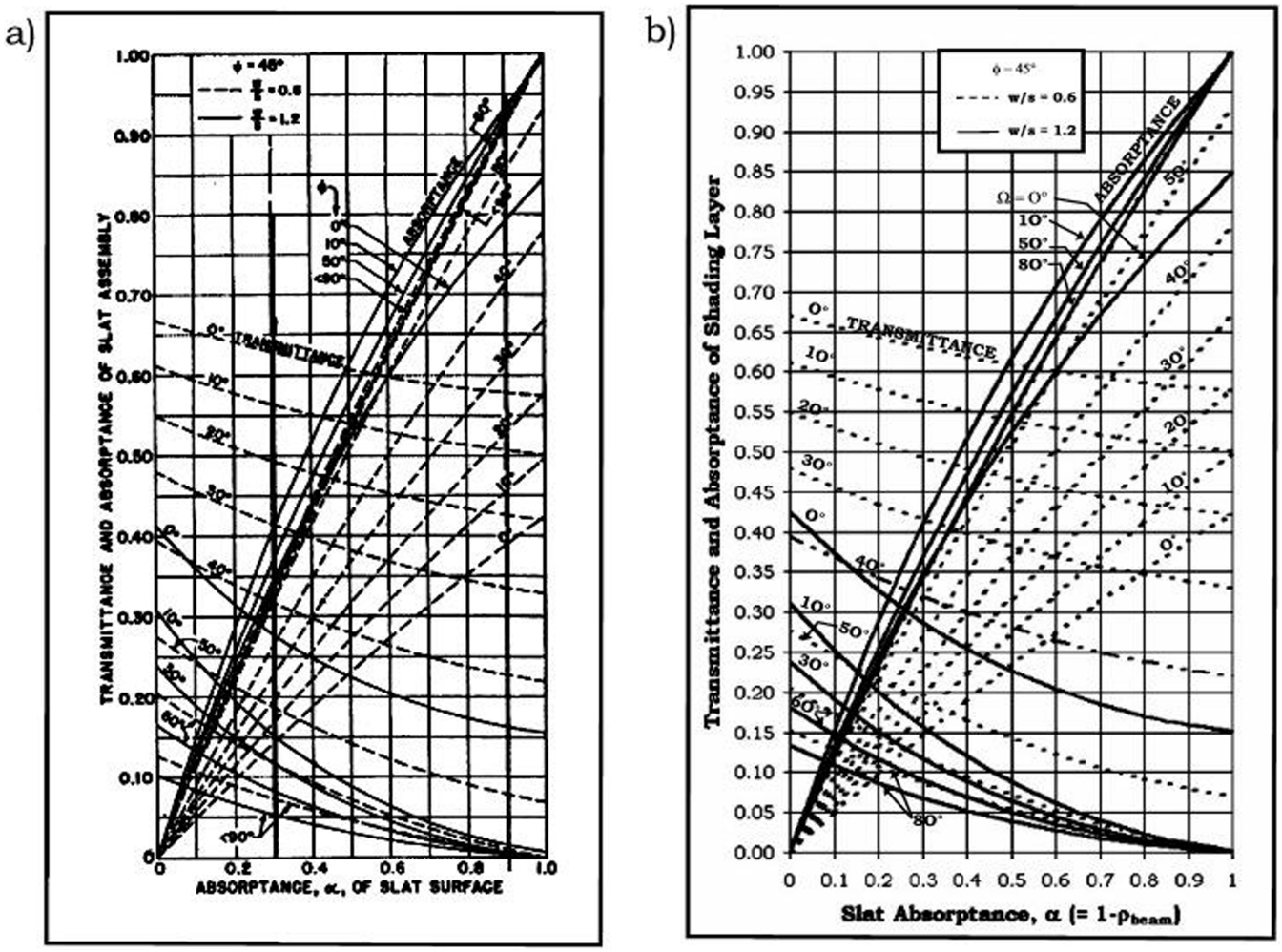

Figure 12 *Transmittance and absorptance of diffuse reflecting slats for monochromatic radiation, ϕ = 45°: (a) Parmelee and Aubele (1952) model, (b) Yahoda and Wright (2004) model.*

Farber, E.A., W.A. Smith, C.W. Pennington, and J.C. Reed. 1963. Theoretical analysis of solar heat gain through insulating glass with inside shading. *ASHRAE Transactions* 69:393-405.

Farber, E.A., W.A. Smith, C.W. Pennington, and J.C. Reed. 1964. Experimental analysis of solar heat gain through insulating glass with indoor shading. *ASHRAE Journal* 6(2):27-39.

Incropera, F.P., and D.P. DeWitt. 1996. *Fundamentals of Heat and Mass Transfer*, 4th ed. John Wiley & Sons.

ISO. 2002. *ISO/DIS 15099, Thermal performance of windows, doors, and shading devices—Detailed calculations*. International Organisation for Standardisation.

Kreith, F., and J.F. Kreider. 1978. *Principles of Solar Engineering*, pp. 53-54. McGraw-Hill.

McCluney, R., and L. Mills. 1993. Effect of interior shade on window solar gain. *ASHRAE Transactions* 99(2):565-570.

Parmelee, G.V., and W.W. Aubele. 1952. The shading of sunlit glass—An analysis of the effect of uniformly spaced flat opaque slats. *ASHVE Transactions*, Vol. 58:377-398.

Parmelee, G.V., W.W. Aubele, and D.J. Vild. 1953. The shading of sunlit glass —An experimental study of slat-type sun shades. *ASHVE Transactions*, Vol. 59:221-240.

Pfrommer, P., K.J. Lomas, and C. Kupke. 1996. Solar radiation transport through slat-type blinds: A new model and its application for thermal simulation of buildings. *Solar Energy* 57(2):77-91.

Rheault, S., and E. Bilgen. 1989. Heat transfer analysis in an automated venetian blind system. *Journal of Solar Energy*, Vol. 111 (Feb.), pp. 89-95.

Rosenfeld, J.L.J., W.J. Platzer, H. Van Dijk, and A. Maccari. 2000. Modelling the optical and thermal properties of complex glazing: Overview of recent developments. *Solar Energy* (Supplement) 69(1-6):1-13.

Rosenfeld, J.L.J., J. Breitenbach, S. Lart, and I. Langle. 2001. Optical and thermal performance of glazing with integral venetian blinds. *Energy and Buildings* 33:433-442.

Wright, J.L. 1998. Calculating center-glass performance indices of windows. *ASHRAE Transactions* 104(1).

Yahoda, D.S. 2002. Calculating effective longwave and solar optical properties of a venetian blind. Master's thesis, University of Waterloo.

Yahoda, D.S., and J.L. Wright. 2004. Methods for calculating the effective longwave radiative properties of a venetian blind layer. *ASHRAE Transactions* 110(1):463-473.